Weight Estimation of Nile Tilapia (*Oreochromis niloticus* Linn.) Using Image Analysis with and without Fins and Tail

Wara Taparhudee and Roongparit Jongjaraunsuk*

ABSTRACT

Manual measurement of live fish is stressful and may cause injuries or post-release mortality. Therefore, indirect measurement based on image analysis should be developed. In this study, 150 Nile tilapia samples of three different size ranges (0.5–1 g, 20–30 g, and 40–60 g·fish^{-1}) were collected. Each fish was photographed five times from above while freely swimming, and then weighed. Data from 1,500 images (10 images of each fish were analyzed: 5 for whole body and 5 without fins and tail) were manually segmented to extract the view area (V). Based on an 80–20 split test, the data were divided into two sets: training data (120 fish; 1,200 images) and validation data (30 fish; 300 images). The results showed that fish body weight (W) fitted with V without fins and tail achieved a higher coefficient of determination (r^2) than whole body. The linear regression model was chosen as the best fit for W estimation based on r^2 (0.922–0.958) and several error analyses: root mean square error (RMSE; 1.02±0.86 g), mean absolute error (MAE; 0.90±0.82 g), mean absolute relative error (MARE; 4.57± 4.11%), maximum absolute error (MXAE; 1.76±1.36 g), and maximum relative error (MXRE; 0.12± 0.10%). Our results indicated that utilizing a linear model was ideal and easy to apply. Furthermore, there is no suffering or weight loss associated with this procedure, since it is not necessary to harvest the fish as with traditional methods. This suggests that the findings of this study can be utilized in a subsequent phase to estimate the weight of freely moving fish, and we also favor incorporating our results with unmanned aerial vehicles (UAVs). Furthermore, Artificial Intelligence (AI) will be employed to identify models capable of autonomous operation.

Keywords: Fish shape, Image analysis, Tilapia, Weight estimation

INTRODUCTION

Nile tilapia (*Oreochromis niloticus* Linn.) is a freshwater fish and the third largest aquaculture product in the world. It is easy to culture and has the advantages of fast growth, physiological strength, and resistance to disease. Nile tilapia farming is carried out in fresh and brackish water environments (Ansari *et al*., 2020; Sgnaulin *et al*., 2020). Efficient Nile tilapia husbandry requires regular measurement of fish weight and length to optimize feed ration. Estimating the weight of fish in ponds, cages or tanks is commonly done by manual measurement. This method results in post-release mortality, physiological stress, potential harm, and other negative effects (Halttunen *et al*., 2010; Stålhammar *et al*., 2012; Gagne *et al*., 2017; Bower *et al*., 2019; McLean *et al*., 2019). Additionally, the amount of feed intake may decrease for several days after weighing, resulting in reduced growth rates (Pickering and Christie, 1981; Maule *et al*., 1989). These effects have been reported for Nile tilapia (Camargo-dos-Santos *et al*., 2021). In addition, manual weighing is labor intensive and time-consuming (Silva *et al*., 2015).

Department of Aquaculture, Faculty of Fisheries, Kasetsart University, Bangkok, Thailand
*Corresponding author. E-mail address: ffisrrj@ku.ac.th
Received 2 March 2023 / Accepted 31 May 2023

To resolve these problems, image analysis has been applied in aquaculture. Balaban *et al*. (2010a) predicted the weight of Alaskan salmon of different species for sorting after harvest (using a light box and motionless specimens), while Torisawa *et al*. (2011) used image analysis with the Move-tr/3DTM software for three-dimensional weight estimation of free-swimming Pacific bluefin tuna (*Thunnus orientalis*) cultured in a net cage. Later, Viazzi *et al*. (2015) developed this technique using computer vision to assess the weight of Jade perch (*Scortum barcoo*) (using a light box and motionless specimens), while Miranda and Romero (2017) developed a prototype using computer vision methods to determine the length of rainbow trout (*Oncorphynchus mykiss*) (a specific measuring prototype). Konovalov *et al*. (2018) and Jongjaraunsuk and Taparhudee (2021) applied image analysis with area measurement to estimate the mass of Asian sea bass (*Lates calcarifer*) (both using a bounding box, but the former with motionless specimens and the latter free-swimming), while Gümüş *et al*. (2021) used image analysis to evaluate the body weight of cultured European catfish (*Silurus glanis*) and African catfish (*Clarias gariepinus*) (light box, motionless specimens). Considering Nile tilapia, Fernandes *et al*. (2020) applied image segmentation techniques using a deep-learning model to identify body regions for weight estimation (using a table-top stand mount and based on carcass traits), while Jongjaraunsuk and Taparhudee (2022) used image analysis for red tilapia (*Oreochromis niloticus* Linn.) weight estimation.

Numerous studies have utilized image analysis, but primarily with images of deceased fish or fish caught under controlled laboratory settings where they are not swimming freely in their natural habitat (e.g., Balaban *et al*., 2010a; Viazzi *et al*., 2015; Konovalov *et al*., 2018; Fernandes *et al*., 2020; Gümüş *et al*., 2021). The image analysis technique developed by Jongjaraunsuk and Taparhudee (2022) has a limited scope of operation. The technique did not evaluate wide-angle images or cover a large area of operation such as a cage for processing.

The current study developed an image analysis method for free-swimming fish to eliminate fish stress from capture and reduce the amount of time involved in manual weighing methods by using the relationship between the top view area and fish weight. The aim was to use this image analysis model as a second step to assess the biomass of fish swimming freely in aquaculture farms under natural conditions.

MATERIALS AND METHODS

Research location and fish sample

One thousand Nile tilapia fry, weighing 0.5–1 g·fish^{-1} were purchased from the Kamphaeng Saen Fisheries Research Station, Faculty of Fisheries, Kasetsart University, Kamphaeng Saen campus, Kamphaeng Saen District Nakhon Pathom Province, Thailand, and transported in two large plastic bags (500 fish·bag^{-1}) to the Freshwater Aquaculture Laboratory, Faculty of Fisheries, Kasetsart University, Bangken, Bangkok, Thailand.

Before starting the experiment, the fish were raised in two 1,000-L tanks (500 fish·tank^{-1}) using a flow-through water system for one week as an acclimatization period. Three air stones were placed in each tank, and the water quality parameters were controlled at appropriate levels for Nile tilapia. Dissolved oxygen (DO), water temperature (Temp), pH, total ammonia nitrogen (TAN), and nitrite-nitrogen (NO_2^-N) were monitored continuously and were maintained in the ranges of 4–7 mg·L^{-1}, 25–32 °C, 7.5–8.5, 0.1–0.5 mg·L^{-1} and 0.1–0.25 mg·L^{-1}, respectively (Azaza *et al*., 2008; Kolding *et al*., 2008; Tran-Duy *et al*., 2012). Fish were fed with 38% protein pelleted feed (Charoen Pokphand Foods Public Co., Ltd.) until satiation twice a day at 9:00 a.m. and 3:00 p.m.

Image acquisition

The experiments were conducted as three consecutive events based on fish size. The first experiment was performed on fish sized 0.5–1 g·fish^{-1} (size 1), whereby 50 healthy fish were taken at random based on their normal swimming behavior and with no visible bodily wounds, and placed in a 50×80×20 cm fiberglass tank containing 80 L of

water with air stones. Then, individual fish were transferred to a white rectangular plastic box (a bounding box) measuring 28×42.2×9.5 cm with a water depth of 7 cm. A ruler was placed beside the box as a calibration scale and all photographs were taken with the ruler included. Photographs were taken at a distance of 80 cm from the lens to the water surface using an Olympus EM 10 Mark II (Olympus Corporation; Tokyo, Japan), at an image size of 4,608×2,592 pixels, with 1/40th sec exposure time and a focal length of 14 mm. Each fish was photographed 10 times, and then weighed using a CST-CDR-3 scale (CST Instruments (Thailand) Ltd.; Bangkok, Thailand) before being returned to an 80–L recuperation tank fully aerated by a sandstone. After recuperation, each fish was returned to the acclimation tank and the fish were reared until they reached the next size ranges (size 2: 20–30 g and size 3: 40–60 g). Each culture period was around three weeks to reach the required sizes. The same procedure applied for size 1 was used for sizes 2 and 3.

Image analysis techniques

Each fish image was refined by using Image J software, National Institute of Health (NIH), USA. This software is an openly accessible (open-source), sovereign platform that supports multiple threads, and it can be used to create user-coded plugins to meet the requirements of any created operation (Stolze *et al*., 2019). The computer used was a Lenovo Legion (running the Windows 10 Home Single Language 64–bit operating system, with an Intel (R) Core (TM) i7-9750H CPU @ 2.60 GHz, 16.0 GB memory (RAM) purchased from Advice IT Infinite Public Co., Ltd. (Bangkok, Thailand).

The procedure for finding the image area to estimate fish weight began by identifying the image of the fish to be analyzed, then selecting the 'segmented' or 'freehand lines' option and marking a straight line on a known object in the image. We used the ruler to draw a 1-cm straight line as mentioned before, then pressed the 'Analyze' button and then 'Set scale' to change the units of length to centimeters and ticked the 'Global' box to apply the scale ratio (Figure 1).

After calibration, 'Polygon selection' was chosen and the mouse was moved around the desired area (around the fish body), clicking to record each segment. Each fish sample was recorded on five photos, and each photo produced an image area of the whole-fish body (selecting fish shape with fins and tail); five images of the fish body were also recorded excluding the fins and tail. Next, we extracted the foreground object from the background and made the fish body black and the background white. This process used image binarizing and a thresholding algorithm (Figure 2). The area of the fish image was calculated by choosing the size option '0–infinity' and circularity as '0–1', and then selecting the 'Analyze particles' option (Figure 3). Pixel area can be calculated from equation 1.

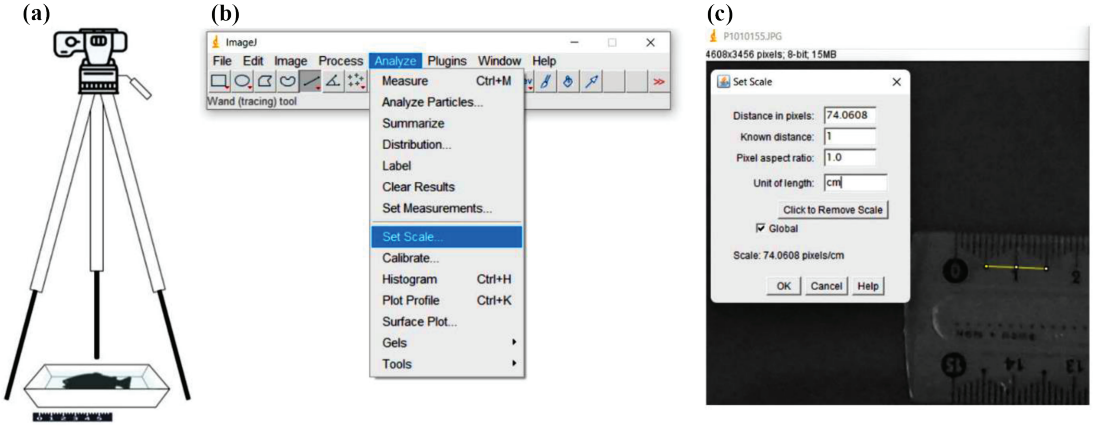

Figure 1. Calibration process: (a) Image acquisition, (b) Set scale, and (c) Set global calibration.

$$\text{Pixel area} = \text{number of pixels} \times \text{scale} \quad (1)$$

Where number of pixels is the total number of pixels within the selected region or the entire image and scale is the physical scale associated with the image. In this study, a 1-cm straight line from a ruler was used. In the case of a processing overview, as shown in Figure 4.

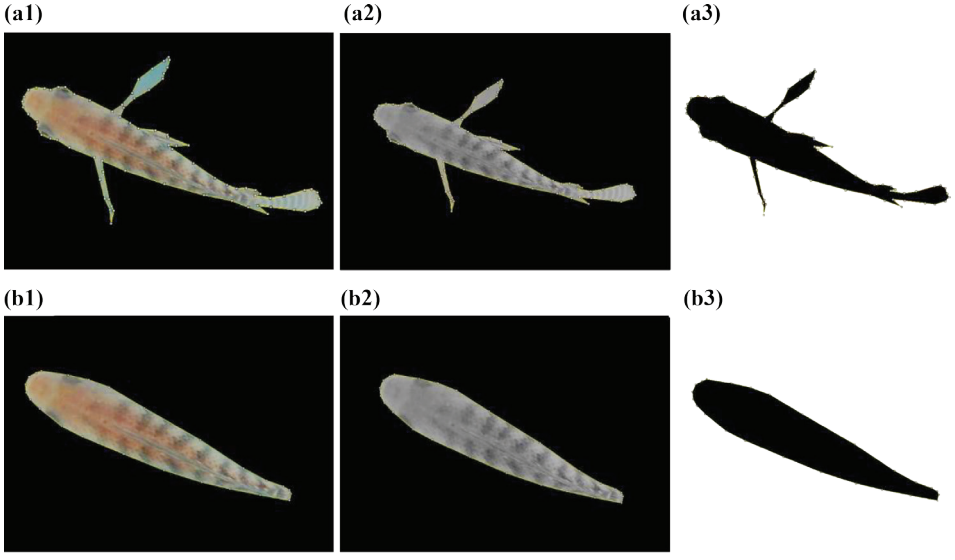

Figure 2. Image extraction for whole fish body (a1, a2, and a3), and fish body excluding fins and tail (b1, b2, and b3).

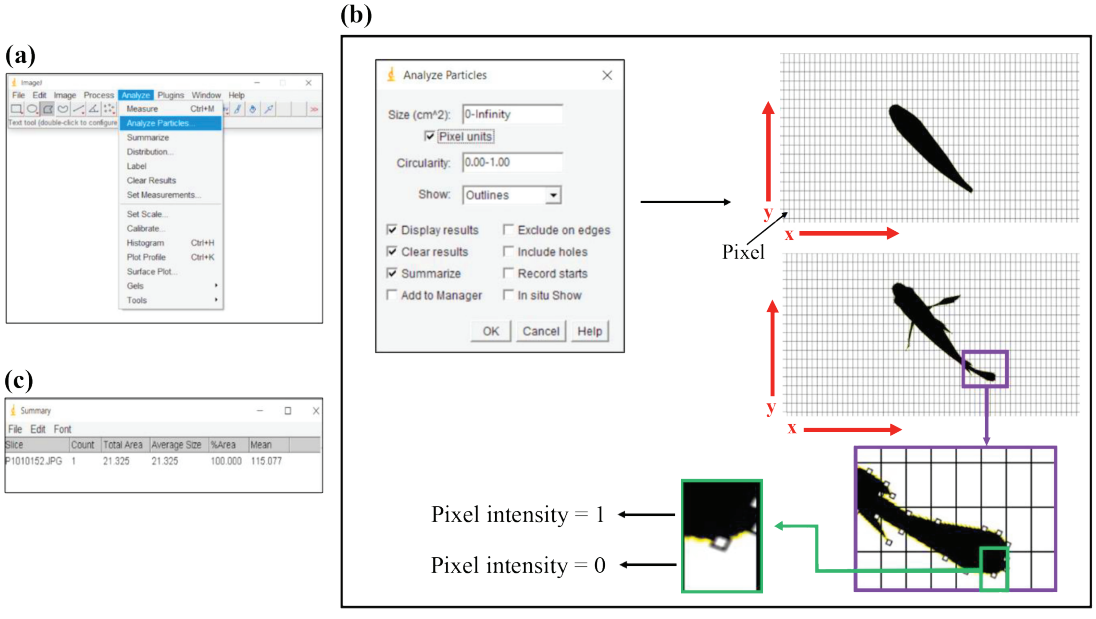

Figure 3. Particle analysis: (a) Analyze options, (b) Analyze particles options; to calculate the size of the pixel area of the fish in the two processing pattens (with and without fins and tail), it can be determined from the total number of black area in the image, and (c) Summary of total area.

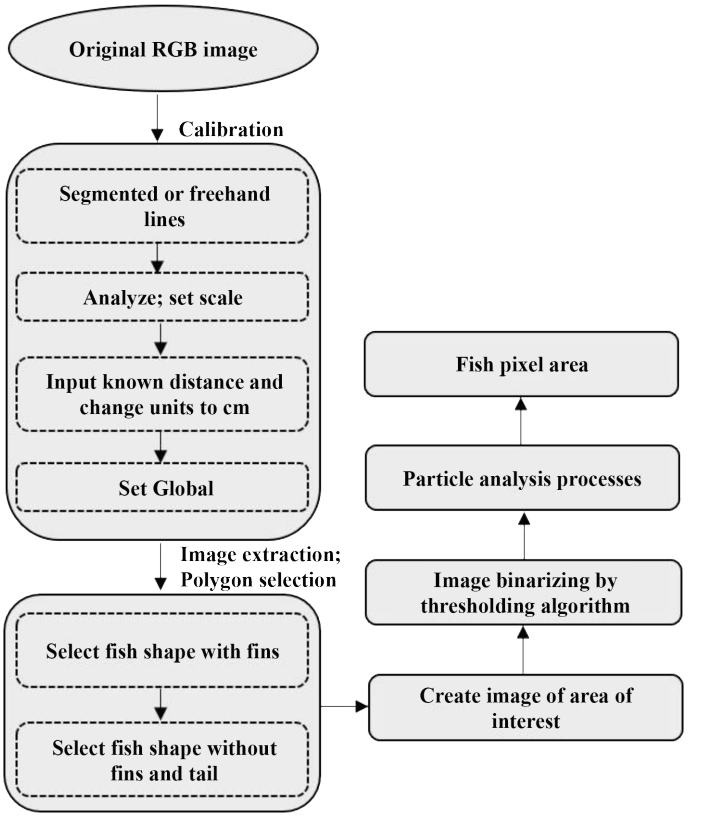

Figure 4. Steps of image processing using Image J software.

Equations for fish weight estimation from images

The relationship between the view area (V) and weight (W) of each fish was generated using mathematical models. Balaban *et al*. (2010a), Zion (2012), Viazzi *et al*. (2015) and Konovalov *et al*. (2018) reported that the mathematical models commonly tested for fish W assessment using real V were linear, power, and polynomial regression models (Equations 2, 3, and 4, respectively).

$$\text{Linear: } W = A+B\,V \quad (2)$$

$$\text{Power: } W = A\,V^{B} \quad (3)$$

$$\text{Polynomial: } W = A+B\,V+C\,V^{2} \quad (4)$$

Where W is the body weight (g), V is the viewable area of the fish (cm^2), and A, B, and C are coefficients.

Ten images of each fish were analyzed (five images for whole body area and five images without fins and tail). To reduce the over-fitting problem, fish image data were divided into two sets using an 80–20% split-test according to Konovalov *et al*. (2018); 80% (40 fish; 400 images) were used as training data and 20% (10 fish; 100 images) were used as out-samples or validation data, as shown in Figure 5.

Data analysis

The body image area per weight and the percentages of fin and tail area to body area of each fish were calculated. The training data set was used to develop the relationship between view area and fish weight to determine the coefficients of determination (r^2) of the linear, polynomial and power models generated from the fish image area of the whole body of the fish (with fins and tail)

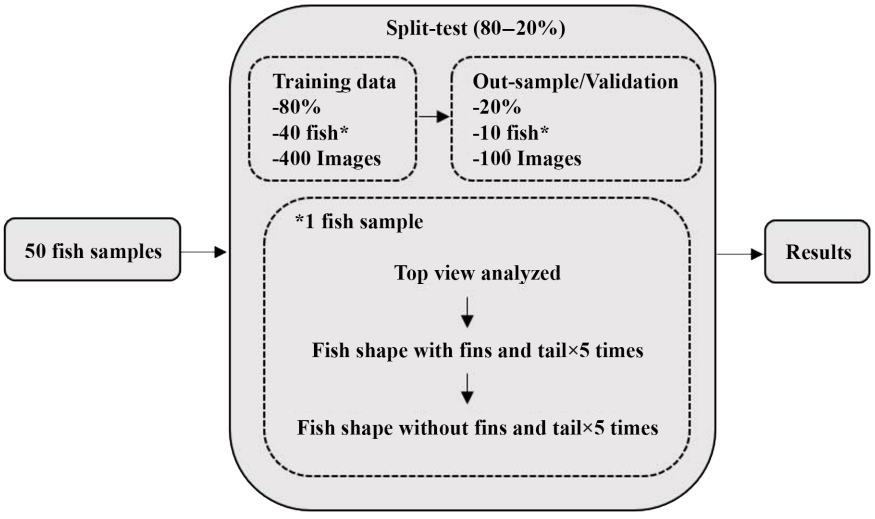

Figure 5. Testing procedure for fish sampling.

and from the fish image area without fins and tail. Then, all the training models were validated for all fish sizes, and average r^2 values were used to compare the models. First, all data were tested for homogeneity using Levene's test of variance. In case of unequal variances, Welch's t-test was applied. If the data were homogeneous, statistical differences were analyzed using an independent sample t-test at a significance level of 0.05. The image acquisition method with the higher r^2 was selected for error analysis using the root mean square error (RMSE), mean absolute error (MAE), mean absolute relative error (MARE), maximum absolute error (MXAE), and maximum relative error (MXRE) statistics for all models, as shown in Equations 5, 6, 7, 8, and 9, respectively.

Root mean square error (RMSE):

$$RMSE = \sqrt{\frac{\sum_{N}^{i=1} [W_{estimated.i} - W_{measured.i}]^2}{N}} \quad (5)$$

Mean absolute error (MAE):

$$MAE = \frac{\sum_{N}^{i=1} |W_{estimated.i} - W_{measured.i}|}{N} \quad (6)$$

Mean absolute relative error (MARE):

$$MARE = \frac{\sum_{N}^{i=1} |W_{estimated.i} - W_{measured.i}| / W_{measured.i}}{N} \times 100 \quad (7)$$

Maximum absolute error (MXAE):

$$MXAE = \max_{i=1}^{N} (|W_{estimated.i} - W_{measured.i}|) \quad (8)$$

Maximum relative error (MXRE):

$$MXRE = \max_{i=1}^{N} \left(\frac{|W_{estimated.i} - W_{measured.i}|}{W_{measured.i}}\right) \quad (9)$$

where $W_{estimated.i}$ represents the estimated weight of each individual, while $W_{measured.i}$ represents the weight obtained from the traditional measuring method.

Then, the average values of each error analysis statistic (RMSE, MAE, MARE, MXAE and MXRE) of each model for each fish size were analyzed for variance differences based on one-way analysis of variance (ANOVA). Mean differences between treatments were compared using Duncan's new multiple range test at the 95% confidence level. All statistical analyses were performed using the IBM SPSS Statistics 26.0 software. Results were presented as the mean±standard deviation (SD).

RESULTS

Relationship between visible area and body weight of fish

In total, 150 fish were examined (50 fish for each size). The results indicated that the body image area (cm^2) per weight (g) increased in fish images both with and without fins and tail. The lowest body weight was 0.40 g and the highest was 63.30 g. When using fish images with fins and tail, the smallest average body image area was 0.98 cm^2 and the largest was 28.49 cm^2, while using images without fins and tail, the smallest average body image area was 0.87 cm^2 and the largest was 24.30 cm^2 (Figure 6).

The largest fish size (size 3) had the highest percentage of fin and tail area to body area (27.83±6.49%) followed by sizes 2 and 1 (21.08± 5.85 and 17.48±6.51%, respectively), as shown in Figure 7.

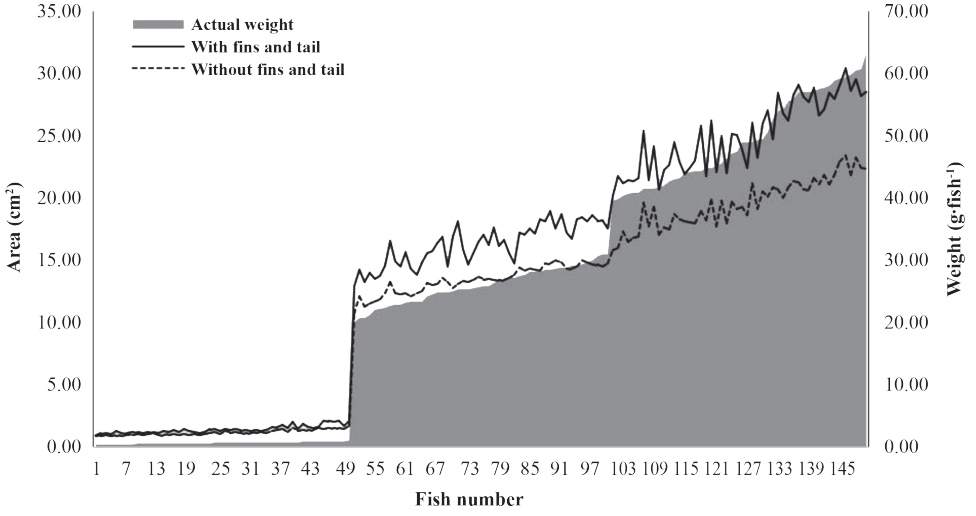

Figure 6. Area of image for each fish weight.

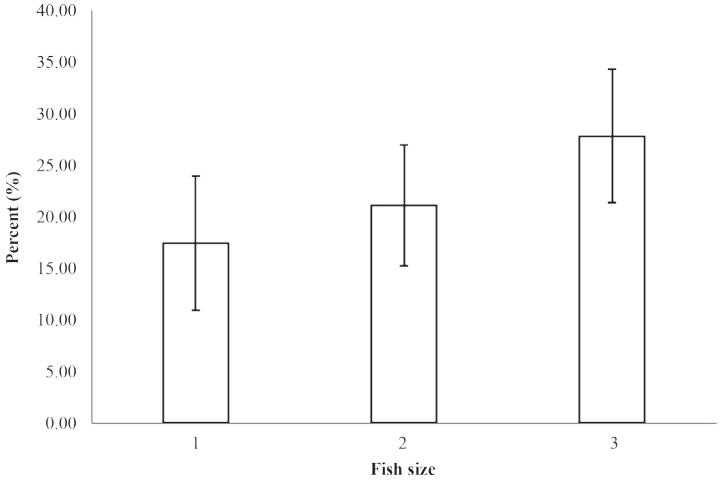

Figure 7. Percentage of fin and tail area to body area of each fish size group (0.5–1 g, 20–30 g, and 40–60 g).
Note: After completing the whole-fish body analysis, each photo was determined individually for the percentage of fin and tail area to body area. Error bars indicate SD.

Training data

The results in Table 1 show that fish images with fins and tail for size 1 (0.55–1 g) yielded r^2 values for the linear, polynomial, and power regression models of 0.902, 0.881, and 0.908, respectively. The same models had r^2 values of 0.930, 0.931, and 0.916 based on fish images without fins and tail. For fish of size 2 (20–30 g), r^2 values for the three models were 0.806, 0.806, and 0.817, respectively, for images with fins and tail, and 0.895, 0.898, and 0.901 for images without fins and tail. For fish of size 3 (40–60 g), r^2 values were 0.802, 0.809, and 0.798 for images with fins and tail, and 0.939, 0.905, and 0.900 for images without fins and tail (Table 1).

Validation

The r^2 values from mathematical models based on image area of the whole fish body and the body without fins and tail were not significantly different ($p>0.05$) for the smallest size group, but were significantly different for the second and third size groups ($p<0.05$). The average r^2 values based on whole fish area and body area without fins and tail were 0.821±0.005 and 0.971±0.018, respectively, for group 2, and 0.754±0.021 and 0.937±0.009 for group 3 (Table 2 and Figure 8a–8c).

The results in Table 2 show that the equations for the fish body image without fins and tail had higher predictive coefficients (r^2) than using the whole-fish body image. Therefore, error analyses were only determined on images without fins and tail. The RMSE, MAE, MARE, MXAE and MXRE values of linear, polynomial and power regression models based on each fish size group were not significantly different ($p>0.05$), as shown in Table 3.

Table 1. Coefficients of area-weight models based on Nile tilapia images with and without fins and tail for three fish size groups.

Size	Weight (g)	Equation	Model coefficients							
			With fins and tail				Without fins and tail			
			A	B	C	r^2	A	B	C	r^2
1	0.5–1	Linear	-0.007	0.497	-	0.902	-0.189	0.761	-	0.930
		Polynomial	-0.304	0.891	-0.124	0.881	-0.051	0.531	0.093	0.931
		Power	0.483	1.043	-	0.908	0.571	1.267	-	0.916
2	20–30	Linear	-0.668	1.609	-	0.806	-7.911	2.515	-	0.895
		Polynomial	0.191	1.501	0.003	0.806	10.306	0.271	0.010	0.898
		Power	1.463	1.024	-	0.817	0.868	1.305	-	0.901
3	40–60	Linear	-8.105	2.290	-	0.802	-23.030	3.740	-	0.939
		Polynomial	45.491	-2.029	0.086	0.809	12.824	0.593	0.064	0.905
		Power	1.232	1.144	-	0.798	1.2774	1.226	-	0.900

Note: A, B, and C are model equation coefficients.

Table 2. Comparison of whole-body fish images and body without fins and tail using three different mathematical models and three size groups of Nile tilapia.

Fish size and model	**Model coefficient (r^2)**		**Levine's test**		**T-test for equality of means**
Fish size: 1 (0.5–1 g)	With fins and tail	Without fins and tail	F	Sig.	Sig. (2-tailed)
Linear	0.929	0.922			
Polynomial	0.941	0.909			
Power	0.954	0.889			
Mean±SD	0.941±0.013	0.907±0.017	0.00	1.00	0.07
Fish size: 2 (20–30 g)					
Linear	0.822	0.958			
Polynomial	0.825	0.963			
Power	0.816	0.991			
Mean±SD	0.821±0.005	0.971±0.018	0.64	0.47	0.04*
Fish size: 3 (40–60 g)					
Linear	0.750	0.937			
Polynomial	0.777	0.929			
Power	0.736	0.946			
Mean±SD	0.754±0.021	0.937±0.009	2.29	0.20	0.00*

Note: * in the row indicates statistical difference at $p<0.05$.

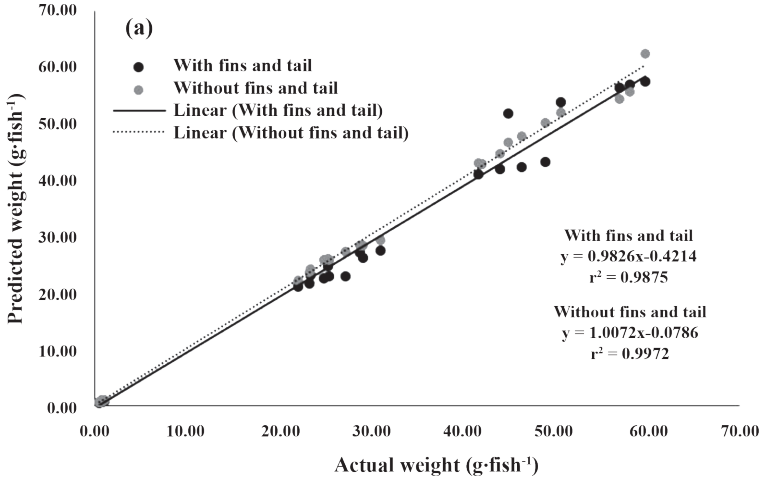

Figure 8. Coefficients of determination (r^2) obtained from three mathematical models of all fish sizes (100 images ·size^{-1}): (a) linear regression model, (b) polynomial regression model, and (c) power regression model.

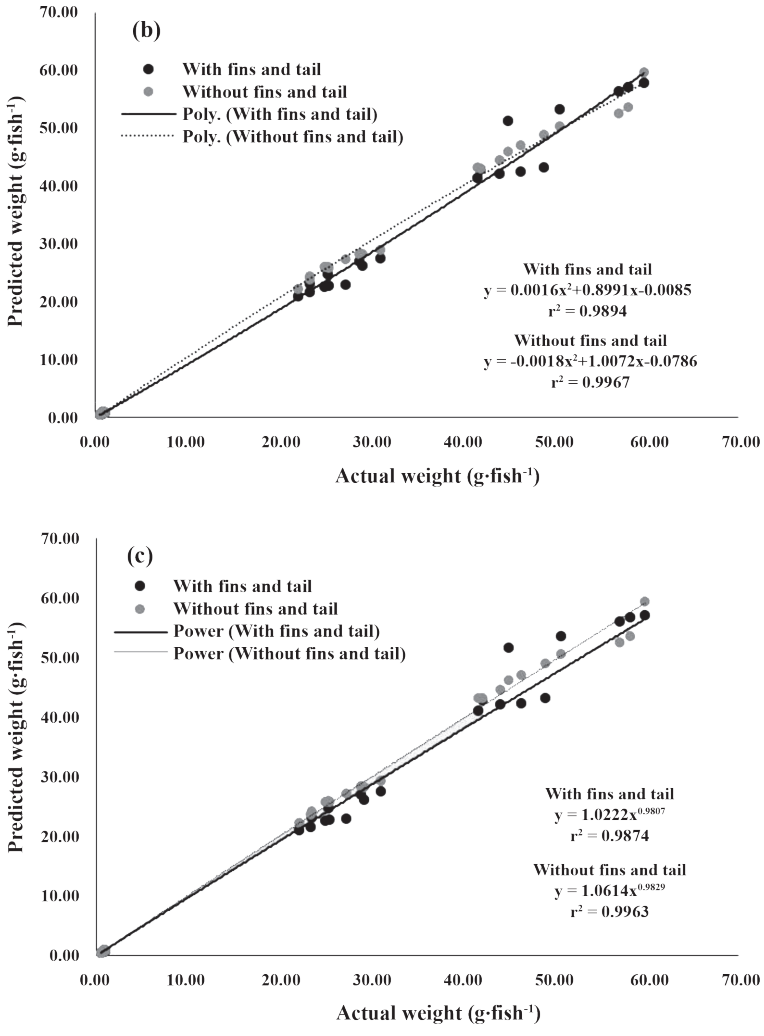

Figure 8. (Continued) Coefficients of determination (r^2) obtained from three mathematical models of all fish sizes (100 images·size^{-1}): (a) linear regression model, (b) polynomial regression model, and (c) power regression model.

Table 3. Error analysis (mean±SD) for mathematical models of images without fins and tail for each fish size group.

Mathematical model	Model			p-Value
	Linear	Polynomial	Power	
RMSE (g)	1.02±0.86	1.30±1.23	1.25±1.20	>0.05
MAE (g)	0.90±0.82	1.08±1.05	1.03±1.02	>0.05
MARE (%)	4.57±4.11	4.85±3.93	4.20±3.11	>0.05
MXAE (g)	1.76±1.36	2.35±2.04	2.28±1.95	>0.05
MXRE (%)	0.12±0.10	0.13±0.09	0.13±0.10	>0.05

DISCUSSION

The results showed that fish weight was positively correlated with fish image area for both the whole-fish image and the body without fins and tail. As fish weight increased, the fish imaging area increased accordingly, concurring with Viazzi *et al*. (2015), Konovalov *et al*. (2018), and Fernandes *et al*. (2020).

The models based on fish body images without fins and tail gave better prediction results than the models using whole-body images. Our results concurred with several other authors who used image processing techniques to assess the weight of a variety of species, including Balaban *et al*. (2010a; Alaskan salmon *Oncorhynchus gorbuscha, O. nerka, O. kisutch, O. keta*), Viazzi *et al*. (2015; Jade perch), Konovalov *et al*. (2018; Asian seabass), Fernandes *et al*. (2020; Nile tilapia), and Jongjaraunsuk and Taparhudee (2021; Asian seabass). Konovalov *et al*. (2018) explained that the fins and tail of the fish had an inconsistent mass due to their high flexibility. They easily deformed during swimming and were often damaged during raising and harvesting. Balaban *et al*. (2010a) suggested that a program should be developed to process the image by cropping the area of the fins and tail. However, Balaban *et al*. (2010b) reported that removing fins and tails did not improve the prediction accuracy of whole Alaskan pollock (*Theragra chalcogramma*) weight based on the view area. The results of the present study indicated that the average r^2 values of all models for the smallest fish with fins included were not significantly different ($p>0.05$) from those without fins, whereas the models did differ in accuracy for the two larger fish groups ($p<0.05$). This might have occurred because percentages of fin and tail area relative to the whole body were smaller for the smallest fish (size 1) than for the larger individuals (sizes 2 and 3).

Most other published mathematical models for fish weight estimation from side-view images used linear or power models. Linear models were applied with grey mullet (*Mugil cephalus*), St. Peter's fish (*Sarotherodon galiaeus*), common carp (*Cyprinus carpio*), Jade perch (*Scortum barcoo*) and Nile tilapia (Zion *et al*., 2012; Viazzi *et al*., 2015; Fernandes *et al*., 2020), whereas power models were applied with Alaskan salmon, (*Oncorhynchus gorbuscha*; *nerka*; *kisutch*; *keta*), Alaskan pollock, (*Theragra chalcogramma*), and Asian seabass (*Lates calcarifer*) (Balaban *et al*., 2010a; 2010b; Konovalov *et al*., 2018). Konovalov *et al*. (2018) suggested that the power model was suitable for large fish.

However, our results applied top-view image analysis, with no apparent statistical differences ($p>0.05$) among all mathematical models. This was possibly because using the top view reduced any problems associated with abnormalities in body or belly shape, which may occur in large fish using image analysis from a side view (Balaban *et al*., 2010a). Therefore, our results suggest that using a linear model is optimal and also simple and easy to apply.

However, due to operational limitations, the developed model application would be unable to assess images from a broad angle or evaluate the entire culture system, particularly in farm ponds or cages in rivers. To resolve these problems, unmanned aerial vehicles (UAVs) could be used to obtain a large-view image. UAVs have been applied in the agricultural sector (on plants) as well as in fisheries for many purposes. Murugan *et al*. (2017) used aerial imagery to provide accurate data for agricultural activities, while Hovhannisyan *et al*. (2018) used a UAV to create a model for appropriate use of farmland. Fisheries applications have included Casella *et al*. (2017), who used UAVs to analyze and assess changes in the structure of shallow coral reefs, Raoult and Gaston (2018), who applied aerial techniques to evaluate the weight, size and number of jellyfish populations to select capture areas and Taparhudee *et al*. (2023), generated a prototype for using UAV with area image analysis for red tilapia weight estimation in river-based cage culture. In the future study, we propose to combine the image processing techniques from this study with UAVs. Additionally, Artificial intelligent (AI) will be employed to identify models capable of running automatically, thereby assisting in further reducing processing time.

CONCLUSION

We have proposed a method to estimate accurately the weight of Nile tilapia by measuring the area of the fish from the top view. Fish shapes without the fins and tail produced better prediction results than fish images with tail and fins. There were no significant differences among the mathematical models investigated. Therefore, our results suggest that using a linear model is optimal and also simple to apply. With our method, the fish do not need to be harvested, and therefore there is no weight loss due to the handling stress incurred using manual weighing procedures.

ACKNOWLEDGEMENTS

The authors appreciate the assistance provided by staff at the Aquacultural Engineering Laboratory. This research was funded by Aquacultural Engineering Laboratory, Department of Aquaculture, Faculty of Fisheries, Kasetsart University, Thailand.

LITERATURE CITED

Ansari, F.A., M. Nasr, A. Guldhe, S.K. Gupta, I. Rawat and F. Bux. 2020. Techno-economic feasibility of algal aquaculture via fish and biodiesel production pathways: a commercial-scale application. **Science of The Total Environment** 704: 135259. DOI: 10.1016/j.scitotenv.2019.135259.

Azaza, M.S., M.N. Dhraïef and M.M. Kraïem. 2008. Effects of water temperature on growth and sex ratio of juvenile Nile tilapia *Oreochromis niloticus* (Linnaeus) reared in geothermal waters in southern Tunisia. **Journal of Thermal Biology** 33(2): 98–105. DOI: 10.1016/j.jtherbio.2007.05.007.

Balaban, M.O., G.F. Unal Şengör, M. Gil Soriano and E. Guillén Ruiz. 2010a. Using image analysis to predict the weight of Alaskan salmon of different species. **Journal of Food Science** 75(3): E157–E162. DOI: 10.1111/j.1750-3841.2010.01522.x.

Balaban, M.O., M. Chombeau, D. Cırban and B. Gümüş. 2010b. Prediction of the weight of Alaskan pollock using image analysis. **Journal of Food Science** 75(8): E552–E556. DOI: 10.1111/j.1750-3841.2010.01813.x.

Bower, S.D., N. Mahesh, R. Raghavan, A.J. Danylchuk and S.J. Cooke. 2019. Sub-lethal responses of mahseer (*Tor khudree*) to catch-and-release recreational angling. **Fisheries Research** 211: 231–237. DOI: 10.1016/j.fishres.2018.11.004.

Camargo-dos-Santos, B., C.L. Carlos, J. Favero-Neto, N.P.C. Alves, B.B. Gonçalves and P.C. Giaquinto. 2021. Welfare in Nile Tilapia production: Dorsal fin erection as a visual indicator for insensibility. **Animals** 11: 3007. DOI: 10.3390/ani11103007.

Casella, E., A. Collin, D. Harris, S. Ferse, S. Bejarano, V. Parravicini, J.L. Hench and A. Rovere. 2017. Mapping coral reefs using consumer-grade drones and structure from motion photogrammetry techniques. **Coral Reefs** 36: 269–275. DOI: 10.1007/s00338-016-1522-0.

Fernandes, A.F.A., E.M. Turra, É.R. de Alvarenga, T.L. Passafaro, F.B. Lopes, G.F.O. Alves, V Singh and G.J.M. Rosa. 2020. Deep Learning image segmentation for extraction of fish body measurements and prediction of body weight and carcass traits in Nile tilapia. **Computers and Electronics in Agriculture** 170: 105274. DOI: 10.1016/j.compag.2020.105274.

Gagne, T.O., K.L. Ovitz, L.P. Griffin, J.W. Brownscombe, S.J. Cooke and A.J. Danylchuk. 2017. Evaluating the consequences of catch-and-release recreational angling on golden dorado (*Salminus brasiliensis*) in Salta, Argentina. **Fisheries Research** 186: 625–633. DOI: 10.1016/j.fishres.2016.07.012.

Gümüş, E., A. Yılayaz, M. Kanyılmaz, B. Gümüş and M.O. Balaban. 2021. Evaluation of body weight and color of cultured European catfish (*Silurus glanis*) and African catfish (*Clarias gariepinus*) using image analysis. **Aquacultural Engineering** 93: 102147. DOI: 10.1016/j.aquaeng.2021.102147.

Halttunen, E., A.H. Rikardsen, E.B. Thorstad, T.F. Næsje, J.L.A. Jensen and Ø. Aas. 2010. Impact of catch-and-release practices on behavior and mortality of Atlantic salmon (*Salmo salar* L.) kelts. **Fisheries Research** 105(3): 141–147. DOI: 10.1016/ j.fishres. 2010.03.017.

Hovhannisyan, T., P. Efendyan and M. Vardanyan. 2018. Creation of a digital model of fields with application of DJI phantom 3 drone and the opportunities of its utilization in agriculture. **Annals of Agrarian Science** 16: 177–180. DOI: 10.1016/j.aasci.2018. 03.006.

Jongjaraunsuk, R. and W. Taparhudee. 2021. Weight estimation of Asian sea bass (*Lates calcarifer*) Comparing whole body with and without fins using computer vision technique. **Walailak Journal of Science and Technology** 18(10): 9495. DOI: 10.48048/wjst.2021.9495.

Jongjaraunsuk, R. and W. Taparhudee. 2022. Weight estimation model for red tilapia (*Oreochromis niloticus* Linn.) from images. **Agriculture and Natural Resources** 56(1): 215–224. DOI: 10.34044/j.anres. 2021.56.1.20.

Kolding, J., L. Haug and S. Stefensson. 2008. Effect of ambient oxygen on growth and reproduction in Nile tilapia (*Oreochromis niloticus*). **Canadian Journal of Fisheries and Aquatic Sciences** 65(7): 1413–1424. DOI: 10.1139/F08-059.

Konovalov, D.A., A. Saleh, J.A. Domingos, R.D. White and D.R. Jerry. 2018. Estimating mass of harvested Asian seabass *Lates calcarifer* from images. **World Journal of Engineering and Technology** 6: 15–23. DOI: 10.4236/wjet.2018.63B003.

Maule, A.G., R.A. Tripp, S.L. Kaattari and C.B. Schreck. 1989. Stress alters immune function and disease resistance in chinook salmon (*Oncorhynchus tshawytscha*). **The Journal of Endocrinology** 120(1): 135–142. DOI: 10.1677/joe.0.1200135.

McLean, M.F., M.K. Litvak, S.J. Cooke, K.C. Hanson, D.A. Patterson, S.G. Hinch and G.T. Crossin. 2019. Immediate physiological and behavioural response from catch-and-release of wild white sturgeon (*Acipenser transmontanus* Richardson, 1836). **Fisheries Research** 214: 65–75. DOI: 10.1016/j. fishres.2019.02.002.

Miranda, J.M. and M. Romero. 2017. A prototype to measure rainbow trout's length using image processing. **Aquacultural Engineering** 76: 41–49. DOI: 10.1016/j.aquaeng.2017. 01.003.

Murugan, D., A. Garg and D. Singh. 2017. Development of an adaptive approach for precision agriculture monitoring with drone and satellite data. **IEEE Journal of Selected Topics in Applied Earth Observations and Remote Sensing** 10(12): 5322–5328. DOI: 10.1109/JSTARS.2017.2746185.

Pickering, A.D. and P. Christie. 1981. Changes in the concentrations of plasma-cortisol and thyroxine during sexual-maturation of the hatchery-reared brown trout, *Salmo trutta* L. **General and Comparative Endocrinology** 44(4): 487–496. DOI: 10.1016/0016-6480 (81)90337-3.

Raoult, V. and T.F. Gaston. 2018. Rapid biomass and size-frequency estimates of edible jellyfish populations using drones. **Fisheries Research** 207: 160–164. DOI: 10.1016/ j.fishres.2018.06.010.

Sgnaulin, T., E.G. Durigon, S.M. Pinho, T. Jerônimo, D.L. de Alcantara Lopes and M.G.C. Emerenciano. 2020. Nutrition of Genetically Improved Farmed Tilapia (GIFT) in biofloc technology system: Optimization of digestible protein and digestible energy levels during nursery phase. **Aquaculture** 521: 734998. DOI: 10.1016/j.aquaculture. 2020.734998.

Silva, T.S.D.C., L.D.d. Santos, L.C.R.d. Silva, M. Michelato, V.R.B. Furuya and W.M. Furuya. 2015. Length-weight relationship and prediction equations of body composition for growing-finishing cage-farmed Nile tilapia. **Revista Brasileira de Zootecnia** 44(4): 133–137. DOI: 10.1590/s1806-92902015000400001.

Stålhammar, M., R. Linderfalk, C. Brönmark, R. Arlinghaus and P.A. Nilsson. 2012. The impact of catch-and-release on the foraging behaviour of pike (*Esox lucius*) when released alone or into groups. **Fisheries Research** 125: 51–56. DOI: 10.1016/j.fishres.2012.01.017.

Stolze, N., C. Bader, C. Henning, J. Mastin, A.E. Holmes and A.L. Sutlief. 2019. Automated image analysis with ImageJ of yeast colony forming units from cannabis flowers. **The Journal of Microbiological Methods** 164: 105681. DOI: 10.1016/j.mimet.2019.105681.

Taparhudee W., R. Jongjaraunsuk, S. Nimitkul and W. Mathurossuwan. 2023. Application of unmanned aerial vehicle (UAV) with area image analysis of red tilapia weight estimation in river-based cage culture. **Journal of Fisheries and Environment** 47(1): 119–131.

Torisawa S., M. Kadota, K. Komeyama, K. Suzuki and T. Takagi. 2011. A digital stereo-video camera system for three-dimensional monitoring of free-swimming Pacific bluefin tuna, *Thunnus orientalis*, cultured in a net cage. **Aquatic Living Resources** 24(2): 107–112. DOI: 10.1051/alr/2011133.

Tran-Duy, A., A.A. van Dam and J.W. Schrama. 2012. Feed intake, growth and metabolism of Nile tilapia (*Oreochromis niloticus*) in relation to dissolved oxygen concentration. **Aquaculture Research** 43(5): 730–744. DOI: 10.1111/j.1365-2109.2011.02882.x.

Viazzi, S., S. Van Hoestenberghe, B.M. Goddeeris and D. Berckmans. 2015. Automatic mass estimation of Jade perch *Scortum barcoo* by computer vision. **Aquacultural Engineering** 64: 42–48. DOI: 10.1016/j.aquaeng.2014.11.003.

Zion, B. 2012. The use of computer vision technologies in aquaculture - A review. **Computers and Electronics in Agriculture** 88: 125–132. DOI: 10.1016/j.compag.2012.07.010.